Research Article

ISSN 2639-9466

Nanotechnology & Applications

Design of Auxetic Structures with Variable Stiffness for Electro-Active Soft Skin Sensor and Actuator

Dong-chan Lee*

IAE, 175-28, Goan-ro 51 beon-gil, Baegam-myeon, Cheoin-gu, Yongin-si, Gyeonggi-do, 17180, Korea.

***Correspondence:**
Dong-chan Lee, IAE, 175-28, Goan-ro 51 beon-gil, Baegam-myeon, Cheoin-gu, Yongin-si, Gyeonggi-do, 17180, Korea.

Received: 08 Apr 2025; **Accepted:** 18 May 2025; **Published:** 26 May 2025

Citation: Dong-chan Lee, Design of Auxetic Structures with Variable Stiffness for Electro-Active Soft Skin Sensor and Actuator. Nano Tech Appl. 2025; 8(1): 1-7.

ABSTRACT

Tendons, which connect muscles to bones, exhibit a distinctive behavior under human physical activity: they become wider and narrower appearing fatter and thinner as they are stretched and contracted. This phenomenon reflects their unusual auxetic behavior, characterized by lateral expansion when stretched longitudinally. Tendons are composed of tough, high-tensile-strength bands of dense fibrous connective tissue. They play a critical role in transmitting mechanical forces generated by muscle contractions to the skeletal system. Especially during abrupt movements such as jumping, tendon dynamics are essential not only for joint positioning and control but also for energy absorption and redistribution. However, tendons are susceptible to damage, particularly under excessive strain or repetitive stress, which often results in injuries. To mitigate such risks and reduce the mechanical burden transmitted through tendons, the development of an auxetic musculoskeletal assistive structure is proposed. This structure utilizes viscoelastic, form-fitting properties, enabling it to simultaneously contract and expand in two perpendicular directions during bodily movements. Such a capability closely mimics the natural auxetic response of tendons, offering both protection and support.

In designing a macro-scale auxetic structure with elastic flexibility suitable for musculoskeletal assistance, it is crucial to develop an auxetic unit cell that allows for adjustable stiffness. This adjustability ensures the structure can adapt to various mechanical demands during motion. Auxetic structures are particularly advantageous in aiding human movement due to their reversible and adaptive configurations, which accommodate dynamic changes in shape and force. Furthermore, the periodic cellular architectures employed in auxetic designs were initially explored in the field of lightweight structural engineering because of their remarkable properties, including high specific stiffness, enhanced damping, and superior energy absorption. These properties now offer promising benefits for biomechanical applications, especially in assistive devices designed to support or augment human musculoskeletal function.

Keywords
Auxetic structure, Cross chiral structure, Variable stiffness, Musculoskeletal assistive structure.

Notation

θ	Tilting angle of strut
S	Deflection curve
α	Bending angle
E_s	Young's modulus of strut
F	Axial forces

Introduction
Tendons are viscoelastic structures that connect muscles to bones, performing the fundamental function of transferring force to and from the skeletal system. They play a critical role in maintaining body positioning and storing elastic energy, especially during abrupt movements such as jumping. However, tendons are also prone to injury, and when damage occurs, it can lead to serious consequences, including permanent loss of function. Injuries such as Achilles tendinopathies, which are common among athletes, are particularly difficult to treat and often require long recovery periods.

Understanding the viscoelastic behavior of tendons is therefore essential, as it may provide insights into protective mechanisms that prevent tissue damage. When relaxed, tendons exhibit a waveform or crimped structure. Stretching at low strain levels results in the straightening of these crimps. Further extension leads to sliding between collagen fibers and fascicles, which eventually return to their original configuration once the load is removed. However, stretching beyond the physiological limit results in permanent deformation and potential tissue damage.

To mitigate such damage and reduce the mechanical load transmitted through tendons, an auxetic musculoskeletal assistive structure is proposed. This structure is designed to conform to body motion through viscoelastic, form-fitting properties, enabling simultaneous contraction and expansion in two perpendicular directions. Such auxetic behavior mimics that of natural tendons and provides dynamic mechanical support.

To design a macro-scale auxetic structure with the flexibility required for musculoskeletal assistance, it is crucial to develop an auxetic unit cell capable of stiffness modulation. Auxetic structures are especially effective in supporting human motion due to their reversible structural configurations. The periodic cellular geometries used in these structures were originally developed in the field of lightweight construction, owing to their high specific stiffness, enhanced damping capacity, and excellent energy-absorbing characteristics [1].

The mechanical performance and deformation behavior of auxetic structures can be tailored by carefully selecting the unit cell geometry [2,3] and adjusting the relative density of the material [4]. These behaviors are governed by a negative Poisson's ratio, wherein a material expands laterally when stretched axially an uncommon trait in most conventional materials.

In this study, auxetic structures composed of various combinations of materials and structural components are investigated. Their potential applications in body protection and biomechanical support systems are explored, focusing on variable stiffness characteristics and user comfort. Finite element analysis (FEA) and experimental evaluations were conducted to assess the performance and effectiveness of the developed auxetic configurations.

Future work includes optimizing the geometric dimensions of the auxetic cells to develop thinner and lighter pad structures without compromising mechanical performance. Auxetic materials, a class of engineered metamaterials that exhibit a negative Poisson's ratio, have been known for over a century but have gained substantial interest only in recent decades. These materials can consist of a single molecular structure or, more commonly, a macroscopic engineered structure with designed mechanical behavior.

Auxetic configurations can be realized using flexure hinge-like or spring-like elements that deform under mechanical loads. Under tensile force, the hinge-like structures extend, leading to lateral expansion; under compressive force, they fold, resulting in lateral contraction. These properties make auxetic materials ideal candidates for adaptive garments and wearable support systems with variable stiffness. Such garments may integrate auxetic material patches, each composed of structured unit cells (as illustrated in Figure 1), that can adapt to motion-induced loads.

To achieve controlled bending behavior, the intermediate layers within the auxetic structure must be constructed as meta-structures, where stiffness can be varied by modulating applied electrical voltage. A constant voltage applied across an electrode layer induces electromagnetic interactions within the spring-like unit cells of the meta-structure, resulting in localized deformation. Variations in this voltage cause changes in stiffness and deformation behavior, enabling electromechanical control over bending.

For experimental validation, a 3D printer (FORMIGA P110, EOS) was used to fabricate auxetic specimens using PEBA2301, a flexible polymer. Mechanical testing was conducted using a universal testing machine (QM100SE, QMSYS) to evaluate the tensile properties and deformation characteristics of the printed auxetic structures.

Design of Auxetic Cell and Experiments

Various designs were developed and evaluated based on key criteria including mechanical performance, user comfort, and manufacturability. Among these, one particular design incorporates an auxetic-patterned structural layer combined with a thin membrane component. This configuration demonstrates high tensile strength while maintaining excellent flexibility in bending and torsion, making it well-suited for dynamic applications involving human movement.

Auxetic materials, a specialized class of metamaterials, derive their unique mechanical behavior from engineered cell geometries that result in a negative Poisson's ratio. This means that when stretched, these materials expand laterally rather than contracting, unlike conventional materials. The structural characteristics and overall mechanical performance of auxetic materials are highly dependent on the design of the unit cell geometry [5-8], allowing for tunable properties based on specific application requirements.

The CCS has a symmetrical geometry and can readily be patterned into a 3D structure with rotation in or out of a plane. Figure 2 shows a structural schematic model in a plane view. The representative unit of CCS is determined by four primary geometrical parameters: length of the strut L, the tilt angle of the strut θ, strut's cross-section in-plane thickness t and width w, as shown in Figure 2. In this study, it is supposed that the cross-sectional shape of struts in CCS is square, so it can be assumed that t=w.

Three configurations are designed for the following compression experiments in the z-direction. For each design, the cubic unit cells are arranged periodically to form 3D lattice samples with 3 × 3 × 3 unit cells. The tilt angle θ of the strut varies from 10 to 30 with the size of the unit cell constant. The models described above are chosen because the geometry of CCS can be varied systematically

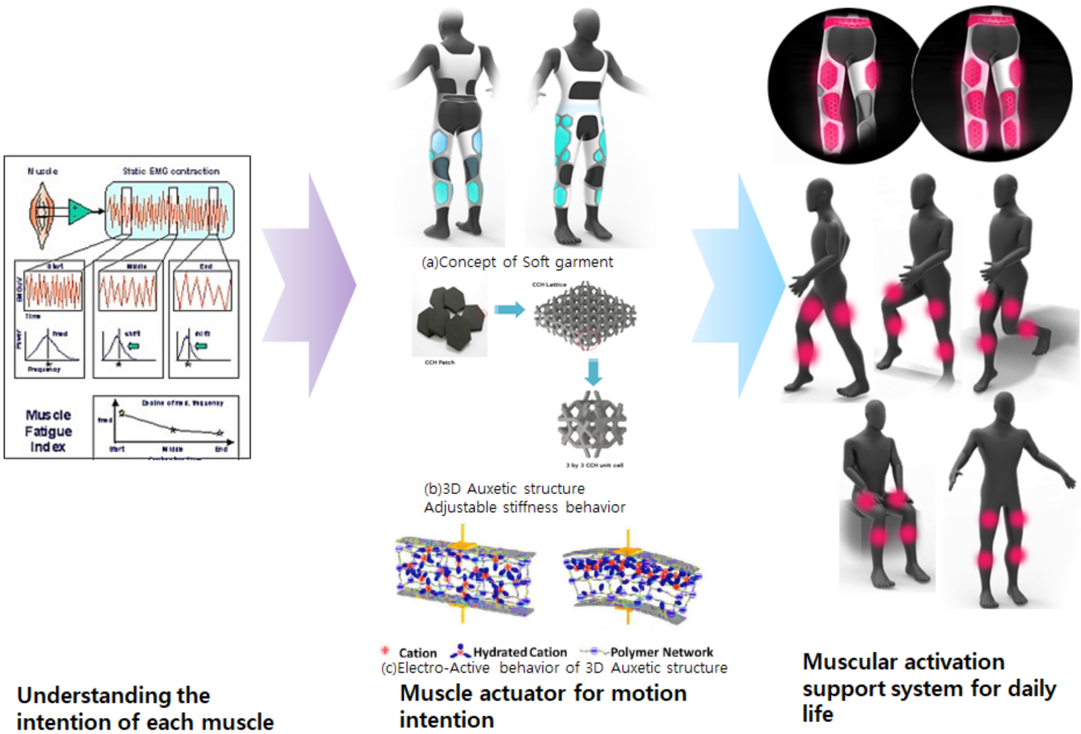

Figure 1: Auxetic musculoskeletal assistive structure with variable stiffness.

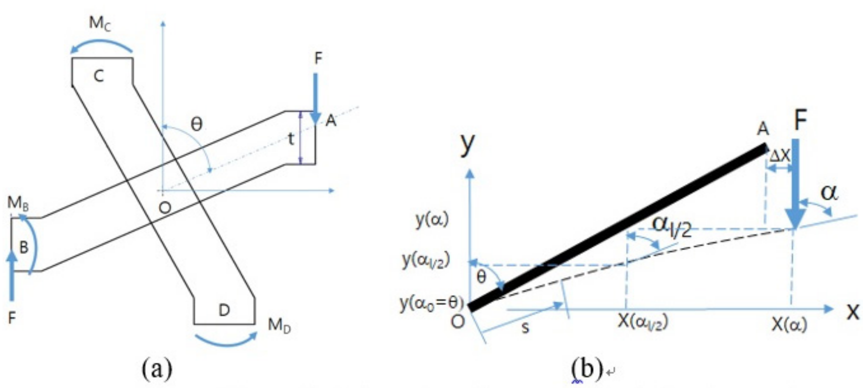

Figure 2: Schematics for cross chiral structure unit.

using a single parameter, θ, which facilitates the analysis of the deformation mechanisms of the auxetic materials. Meanwhile, the size of each model needs to meet the requirements for fabrication and experiments. The force analysis of the representative unit at the top or bottom layers is shown in Figure 2. The end-point A is the free end, which is only contacted with the hard striker. But, due to the symmetry of the structure, constraints at the end-points B, C, and D are much stronger because of the rigid connection with other units. As a result, the main deformation occurs in strut-OA while slight deformation is observed in other struts. Therefore, the deformation of the struts-OB, OC, and OD can be neglected, and strut-OA is simplified to a cantilever beam where the origin O is fixed in this model.

The bending moment and axial stress at origin O can be expressed as,

$$M_O = \frac{FLsin\theta}{2}, \sigma_a = \frac{FLcos\theta}{t^2} \quad (1)$$

The model regarding large deflection takes nonlinear dimensional change into consideration and it is expected to be more accurate in calculating the value of stress in a typical position. Before reaching the plastic yield stress, the strut is subjected to large deflection upon loading, which could affect the stress distribution, as shown in Figure 2-b. The model regarding large deflection takes nonlinear dimensional change into consideration and it is expected to be more accurate in calculating the value of stress in a typical position. Additionally, the perfectly plastic beam is also used and several assumptions are adopted for theoretical analysis: the large deformation is analyzed in the elastic section of the material and the process will not be considered that the failure occurs at the surface first and then extends across the entire section when the strut starts to yield.

In Figure 2-(b), a curvilinear coordinate S, with origin O, is used to define the position of the bending member. Neglecting the change in length of OA due to axial compression. According to the Euler-Bernoulli theorem for beam bending, the differential equation of the deflection curve is,

$$\frac{d\alpha}{ds} = \frac{M(x)}{E_S I} = \frac{F\left(\frac{L}{2}sin\theta + \Delta x - x\right)}{E_S I} \qquad (2)$$

where I is second moment inertia of the cross-section and $I = {wt^3}/{12}$, α is the bending angle of a general point along a deformed member between the tangent of the shape of the inclined member and the loading direction, Δ*x* is the maximum lateral displacement before the strut fails, *s* and *x* are the distances of a general point along the curvilinear coordinate and along the horizontal direction from origin O, respectively. Considering the relationship between the O-*xy* and O-*s* coordinate systems, the following geometrical relationships could be readily obtained,

$$dx/ds = sin\alpha, \; dy/ds = cos\alpha, \qquad (3)$$

Differentiating Eq. (2) with respect to *s* and combining Eq. (3), we obtain,

$$d^2\alpha/ds^2 = \frac{F}{E_S I}\frac{dx}{ds} = -\frac{F}{E_S I}sin\alpha \qquad (4)$$

Using Eq. (4), the following equation can be yield,

$$\left(\frac{d^2\alpha}{ds^2}\right)\cdot\frac{d\alpha}{ds} = -\frac{F}{E_S I}\cdot sin\alpha\cdot\frac{d\alpha}{ds} \qquad (5)$$

Eq. (5) may be integrated once to yield,

$$\frac{1}{2}\left(\frac{d\alpha}{ds}\right)^2 = \frac{F}{E_S I}\cdot cos\alpha + c \qquad (6)$$

where the boundary conditions is,

$$\alpha|_{s=0} = \theta, \frac{d\alpha}{ds}\Big|_{s=0} = \frac{M|_{x=0}}{E_S I}\;, \alpha|_{s=L/2} = \alpha_{L/2}, \frac{d\alpha}{ds}\Big|_{s=L/2} = 0 \qquad (7)$$

and then

$$c = \frac{F}{E_S I}cos\alpha_{L/2}, \; M|_{x=0} = \sqrt{2FE_S I\left(cos\alpha_0 - cos\alpha_{L/2}\right)}, \qquad (8)$$

It can be seen form Figure 1-(b) that $d\alpha/ds$ is positive, solving for *ds* gives,

$$ds = \sqrt{\frac{E_S I}{2F}}\cdot\frac{1}{\sqrt{\left(cos\alpha_0 - cos\alpha_{L/2}\right)}}d\alpha \qquad (9)$$

Performing one more integration of Eq. (9) yields,

$$\frac{L}{2} = \sqrt{\frac{E_S I}{2F}}\cdot\int_{\alpha_0}^{\alpha_{L/2}}\frac{1}{\sqrt{\left(cos\alpha_0 - cos\alpha_{L/2}\right)}}d\alpha \qquad (10)$$

From eq. (10), the force F can be expressed as,

$$F = \frac{2E_S I}{L^2}\cdot\left[\int_{\alpha_0}^{\alpha_{L/2}}\frac{1}{\sqrt{\left(cos\alpha_0 - cos\alpha_{L/2}\right)}}d\alpha\right]^2 \qquad (11)$$

For these bending-dominated cell structures, the yield stress is obtained by setting the moment equal to the collapse moment in the critical struts. If the fully plastic behavior for a perfectly plastic beam under combined bending moment and extensional stress can be estimated, the loading conditions may be predicted for the bending angle of a general point along a deformed member between the tangent of the shape of the inclined member and the loading direction.

Using Eqs. (3) and (9), the horizontal projected distance *x(α)* of a general point (*x, y*) on the strut-OA along the *x*-axis and the vertical projected distance *y(α)* of the general point (*x*, *y*) along the *y*-axis can be estimated.

Figure 3 shows a unit cell and lattice structure for the behaviors of CCS. The cross-chiral auxetic structure has a symmetrical geometry, as shown in Figure 2. After rotation in the out-of-plane direction, this 2D structure can be readily patterned into a 3D structure, CCS, as shown in Figure 3.

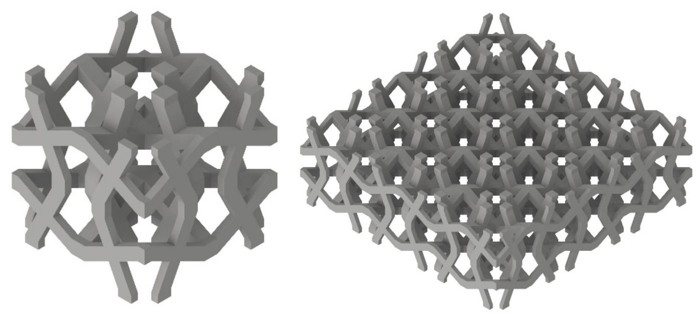

(a) Unit cell of cross chiral structure

(b) 3 by 3 lattice of cross chiral structure

Figure 3: 3D models of cross chiral structure.

Results and Discussion

Auxetic cells fabricated using polyurethane (as presented in Table 1) exhibit a negative Poisson's ratio, and their auxetic behavior is influenced significantly by the geometric parameters of the unit cell. Each auxetic block has dimensions of 30 mm × 30 mm × 10 mm, as shown in Figure 4(a). The specimens are designed with varying tilting angles of the unit cells to investigate the effects of geometry on structural performance.

For enhanced comparative analysis, the fabricated specimens were doubled in width and height while maintaining a constant thickness. A key mechanical property evaluated in these experiments is the compressive strength, defined as the maximum stress a material can endure under compression before failure or fracture. This characteristic is particularly important for auxetic materials, as shown in Figure 4(b).

The compression test setup was conducted using a universal testing machine (QM100SE, QMSYS), following a standardized testing protocol that includes procedures for sample preparation, fixturing, gauge length specification, and data analysis. During testing, the specimen is securely mounted between the grips of the machine. An extensometer is attached to monitor the change in gauge length throughout the compression process. In the absence of an extensometer, the testing machine itself records displacement data by tracking the relative movement of its crossheads, which hold the specimen.

Once the test begins, a gradually increasing compressive load is applied to the specimen. The maximum payload applied during testing can reach up to 40 kgf, as illustrated in Figure 4(c). This setup enables accurate assessment of the deformation behavior and strength of the auxetic samples under load, providing insight into the relationship between cell geometry and mechanical performance.

Table 1: Material properties of auxetic cell.

Characteristics	Unit	Polyurathane (Semiflex)
Density	kg/m3	1200
Tensile Modulus	MPa	15.30-25.82
Shear Modulus	MPa	3.27-8.38
Poisson's Ratio	-	0.48
Tensile Strength	MPa	23

Figure 4 shows various auxetic structure specimens. Sample 1 is CCS (cross-chiral structure) structure with the top and bottom plates that is to protect the warping behaviors of auxetic cells and sample 2 is a CCS structure without them. In this paper, sample 2 is selected as the valid prototype for the soft auxetic structure with variable stiffness [5-8]. Figure 5 shows the stress-strain curve on

(specimen 1) (specimen 2) (specimen 3)

(a) Auxetic structure specimens

(b) Compression test using universal tensile machine

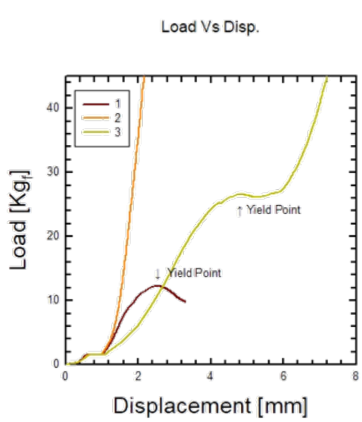

(c) Force-displacement curve of specimen 1, 2, and 3

Figure 4: Test specimens and machine for the structural properties of an auxetic unit cell.

the rotation variable (θ) of the CCS bridge. As the lower rotation angle is applied, more resistance capacity and faster inflection are observed. The collapse of the CCS structure occurs at around 20 degrees of the strut angle θ. Under 10 degrees, the structure possesses a linear behavior. When a more obvious inflection range exists, clearer changes in strength and flexibility can be observed and the external force absorption is expected to be excellent. Over 30 degrees, it is similar to a solid block from the beginning of external force and does not show the structural characteristics of CCS.

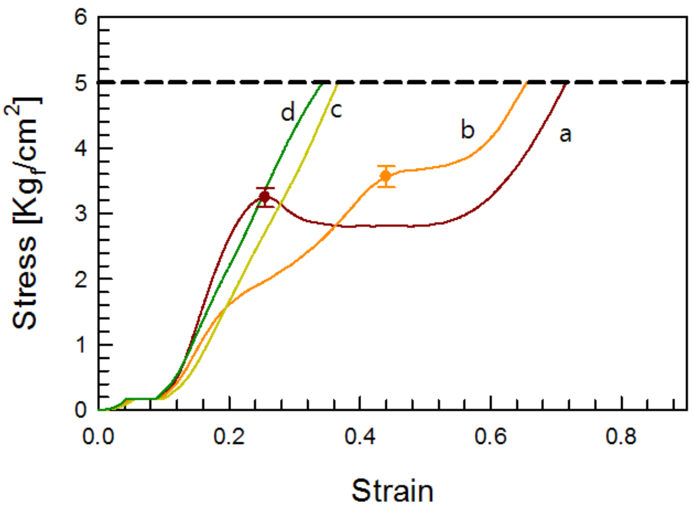

Figure 5: Stress-strain curve of CCS (a: 10 degree, b: 20 degree, c: 30 degree, d: 40 degree) UTM results is given by solid lines; symbols denote yield points; the chain line represent our reference value, 5.

Using the auxetic sample 2 of 3x3 CCS structure, the stress-strain curve, and strain coefficient are shown in Figure 6 and 7 for the compression ratio (compressibility) percentages (a. 0%, b. 20%, c. 30%, d. 40%). Those figures show the average values obtained from five experiments for each sample, in which the solid line shows the experimental value of the universal testing machine and the symbol depicts the inflection point on the structural change or analogical yielding point (5 kgf/cm2). Except for the analogical yielding phenomenon of the specimen with 0% compressibility, others have more yielding points in the test range. This analogical yielding point increases as the compressibility increases. The mechanical characteristics of CCS gradually disappear at the 40% compression rate, which means a physical property becomes similar to the solid structure as shown in Figure 6.

Figure 7 illustrates the strain coefficient related to compressibility, which is represented as the slope of the stress strain curve. This strain coefficient reflects the material's resistance to external compressive forces and its inherent mechanical strength. In the graph, the inverted triangle and triangle markers respectively represent the slopes before and after the inflection point on the stress–strain curve. The dash-dot line indicates the difference between these two slope values. The initial mechanical properties of the auxetic pad are largely determined by the pre-inflection slope (inverted triangle), while the resistance to external compression is influenced by the post-inflection slope (triangle).

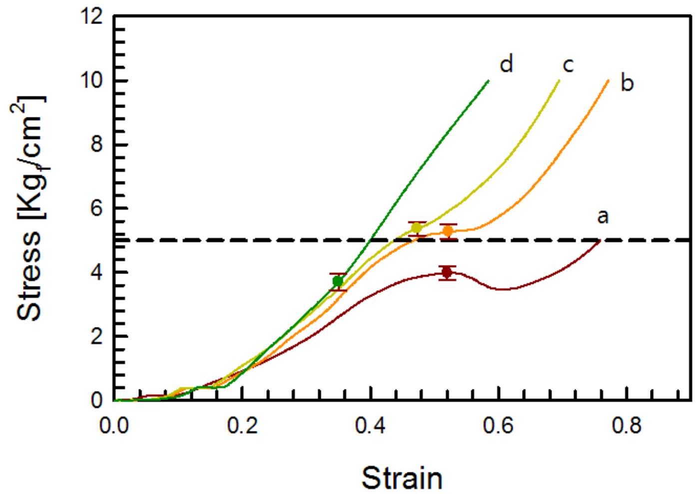

Figure 6: The stress to CCS structure as a function of strain for a: non-compression, b: 20%-compression, c: 30%-compression, d: 40%-compression. UTM results is given by solid lines; symbols denote yield points; the chain line represent our reference value, 5

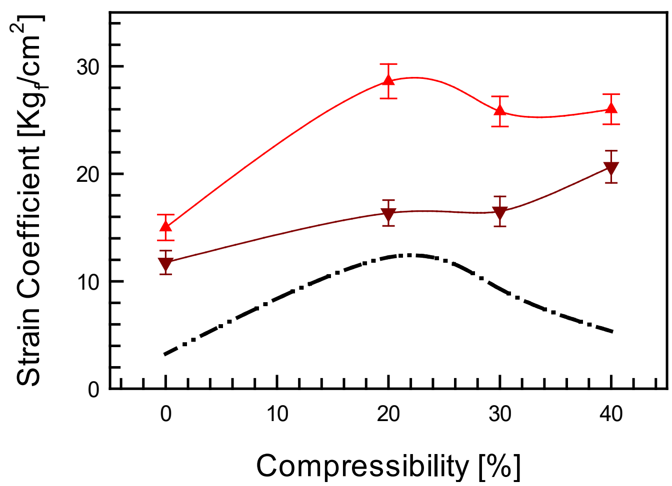

Figure 7: Strain coefficient as a function of compressibility: 20% compression (top orange curve), 30% compression (middle brown curve), and 40% compression (bottom single point curve).

The buckling behavior observed in auxetic pads results in a 20% change in compressibility, which is dependent on the structural configuration of the Cross-shaped Cellular Structure (CCS). It is estimated that the maximum variation in compression rate could reach 22%, indicating the structure's sensitivity to geometrical changes under load. Additionally, the curves for Poisson's ratio and stiffness exhibit high nonlinearity with respect to changes in unit cell dimensions. This nonlinear behavior arises from the variability in cell stiffness and the surface contact interactions between struts. During gradual compression, the individual cell components remain relatively rigid due to their high stiffness, and only the vertical struts begin to buckle and collapse, initiating surface contact between structural elements.

As compression continues, the auxetic hollow structure transitions into a more densely packed solid structure, which begins to behave like a conventional material with diminished auxetic properties. Conversely, under tensile loading, the zigzag-shaped vertical struts begin to straighten, absorbing the load, while the rhombus-shaped elements undergo minimal deformation. This behavior marks the transition from an auxetic to a non-auxetic (normal) structure, with the onset of surface contact during compression, and full straightening of the vertical struts under tension, serving as key indicators of this structural shift.

Conclusion

The Cross-shaped Cellular Structure (CCS) demonstrates a strong capacity to regulate its mechanical properties across a wide range by adjusting its geometric parameters or relative density. Moreover, the CCS exhibits stable auxetic behavior even under large deformations, enabling the predictable deformation response in such conditions.

Experimental results indicate that the CCS with a tilting angle (θ) of 30° possesses the highest energy absorption capacity. Under quasi-static (low-velocity) and medium-velocity loading conditions, Sample 2 maintains a stable energy absorption efficiency of approximately 50%, which surpasses that of most previously reported cellular materials. Notably, Sample 2 shows the highest energy absorption efficiency under quasi-static loading conditions, indicating superior performance in applications requiring passive impact protection or energy dissipation.

The strut thickness plays a critical role in influencing the variable stiffness behavior of auxetic cells. To achieve soft variable stiffness within the auxetic unit under an applied load, the resistance to deformation must be precisely controlled by adjusting the strut angle and thickness. For application in macro-scale auxetic structures, such as wearable variable stiffness suits, it is recommended that the geometric response follows a negative slope meaning that the structure becomes stiffer beyond a certain strut angle, and more flexible below it.

Therefore, valid ranges of strut angle, thickness, and length should be carefully determined for a given load condition. These findings result from the unique design of soft auxetic unit cells, fabricated using various materials. During the initial phase of the compression test, the stress–strain curve displays a low elastic modulus, which increases significantly once the deformation is transferred to the auxetic material. This behavior allows for the observation of distinct differences between the compressive strength and the elastic modulus.

The elastic modulus was specifically analyzed from the moment the force began to act directly on the material, while compressive strength was defined as the maximum stress value at 30% strain. These measurements provide crucial insights into the mechanical response characteristics and the stiffness evolution of the auxetic structure under loading.

Acknowledgement

This work was supported by the Technology Innovation Program (20019115) funded by the Ministry of Trade, Industry, & Energy (MOTIE, Korea).

References

1. LJ Gibson, MF Ashby. Cellular Solids: Structure and Properties. Cambridge: Cambridge University Press, 2 edition. August 13, 1999.
2. A Woesz, J Stampfl, P Fratzl, et al. “Cellular solids beyond the apparent density-an experimental assessment of mechanical properties”. Adv. Eng. Mater. 2004; 6: 34-138.
3. SJ Li, QS Xu, Z Wang, et al. “Influence of cell shape on mechanical properties of Ti-6Al-4V meshes fabricated by electron beam melting method”. Acta. Biomater. 2014; 10: 4537-4547.
4. MF Ashby. “The properties of foams and lattices”. Pil Trans R Soc. 2006; 364: 15-30.
5. T Bückmann, R Schittny, M Thiel, et al. “On three-dimensional dilational elastic metamaterials”. New J. Phys. 2014; 16: 33032.
6. T Bückmann, N Stenger, M Kadic, et al. “Tailored 3D mechanical metamaterials made by dip-in direct-laser-writing optical lithography”. Adv. Mater. 2012; 24: 2710-2714.
7. R Critchley, I Corni, JA Wharton, et al. “The preparation of auxetic foams by three-dimensional printing and their characteristics”. Adv. Eng. Mater. 2013; 15: 980-985.
8. MS Rad, Y Prawoto, Z Ahmad, et al. “Analytical solution and finite element approach to the 3D re-entrant structures of auxetic materials”. Mech. Mater. 2014; 74: 76-87.